Rotordynamic Effects Driven by Fluid Forces from a Geometrically
Imperfect Labyrinth Seal

by

William C. Williston, Jr.
Lieutenant , United States Navy
B.S.M.E., United States Naval Academy, 1983

Submitted in partial fulfillment of
requirements for the degree of

MASTER OF SCIENCE IN MECHANICAL ENGINEERING

from the

NAVAL POSTGRADUATE SCHOOL
December 1993

REPORTS DOCUMENTATION PAGE

1a Report Security Classification Unclassified		1b Restrictive Markings		
2a Security Classification Authority		3 Distribution Availability of Report Approved for public release; distribution unlimited.		
2b Declassification/Downgrading Schedule		5 Monitoring Organization Report Number(s)		
6a Name of Performing Organization Naval Postgraduate School	6b Office Symbol (If Applicable) ME	7a Name of Monitoring Organization Naval Postgraduate School		
6c Address (city, state, and ZIP code) Monterey , CA 93943-5000		7b Address (city, state, and ZIP code) Monterey, CA 93943-5000		
8a Name of Funding/ Sponsoring Organization	8b Office Symbol (If Applicable)	9 Procurement Instrument Identification Number		
8c Address (city, state, and ZIP code)		10 Source of Funding Numbers		
Program Element Number	Project No.	Task		Work Unit Accession No.

11 Title (Include Security Classification)
Rotordynamic Effects Driven by Fluid Forces From a Geometrically Imperfect Labyrinth Seal

12 Personal Author(s)
William C. Williston, Jr.

13a Type of Report Master of Science Thesis	13b Time Covered From To	14 Date of Report (year, month, day) December 1993	15 Page count 43

16 Supplementary Notation The views expressed in this thesis are those of the author and do not reflect the official policy or position of the Department of Defence or the U. S. Government.

17 Cosati Codes:	Field	Group	Subgroup

18 Subject Terms (continue on reverse if necessary and identity by block number)
Residual Vibrations, Linear Perturbation, Lumped Parameter, Fluid Forces, Mass Unbalance

19 Abstract (continue on reverse if necessary and identity by block number)

    The forces on a rotor due to asymmetric pressure distributions resulting from a single gland non-circular labyrinth seal in a circular outer casing are analyzed for the purpose of understanding the possible causes of synchronous vibration due to seal intolerance. A lumped parameter model is developed for flow in the azimuthal direction inside the seal gland. The sealing knife imperfections causing the non-circularity may be due to manufacturing defects or in service ware. The resulting continuity and momentum equations are solved using a regular linear perturbation technique. Results from this model indicate under what conditions seal imperfections can generate forces of the same order of magnitude as rotor mass unbalance.

20 Distribution/Availability of Abstract X unclassified/unlimited same as report DTIC users	21 Abstract Security Classification Unclassified	
22a Name of Responsible Individual Professor K. Millsaps	22b Telephone (Include Area Code) (408) 656-3382	22c Office Symbol ME-MI

ABSTRACT

The forces on a rotor due to asymmetric pressure distributions resulting from a single gland non-circular labyrinth seal in a circular outer casing are analyzed for the purpose of understanding the possible causes of synchronous vibration due to seal intolerance. The sealing knife imperfections causing the non-circularity may be due to manufacturing defects or in service ware. A lumped parameter model is developed for flow in the azimuthal direction inside the seal gland. The resulting continuity and momentum equations are solved using a regular linear perturbation technique. Results from this model indicate under what conditions seal imperfections can generate forces of the same order of magnitude as those arising from residual rotor mass unbalance.

TABLE OF CONTENTS

LIST OF FIGURES

LIST OF SYMBOLS

A_1 Gland inlet area

A_c Circumferential area of gland

$C = \dfrac{q^*}{\rho^* \delta_1^* V^*}$ Nondimensional flow rate parameter

$D = 1 - \dfrac{V_i}{V^*}$ Nondimensional swirl change parameter

D_h Hydraulic diameter of gland inlet area

h_1 Mean height of gland knives

l Distance between sealing knives

$P = P^*(1 + \xi)$ Total pressure upstream of seal

P_o Static pressure down stream of second knife

P^* Zeroth order static pressure inside gland

q_1 Inlet mass flow per unit length

q_2 Outlet mass flow per unit length

q^* Zeroth order mass flow per unit length

R_a Air gas constant (287.15 J/kg K)

Re_R Rotor Reynolds number

Re_S Stator Reynolds number

R_s Mean radius of stator

T Mean temperature

$V = V^*(1 + \eta)$ Swirl velocity in the seal gland

V_i Inlet swirl velocity

V^* Zeroth order swirl velocity (θ-direction) inside of gland

δ_1 Local radial clearance between stator and first knife

δ_1^* Circumferential average gap for stator and first knife

δ_2 Local radial clearance for stator and second knife

δ_2^*	Circumferential average gap for stator and second knife
ε_1	Inlet seal gap perturbation magnitude - first harmonic
ε_2	Outlet seal gap perturbation magnitude - first harmonic
ε_3	Gland depth perturbation amplitude - first harmonic
ϕ_1	Phase angle of the 1st harmonic inlet gap perturbation
ϕ_2	Phase angle of the 1st harmonic exit gap perturbation
ϕ_3	Phase angle of the 1st harmonic gland depth perturbation
θ	Angular coordinate in absolute reference frame
ρ	Density of fluid inside of the seal gland
η	Velocity perturbation
ξ	Pressure perturbation
λ_r, λ_s	Darcy friction factors for rotor and stator respectively
μ_1	Flow coefficient for first sealing gap
μ_2	Flow coefficient for second sealing gap

I.   INTRODUCTION

The United States Navy has extensive experience with gas turbine engines in aviation applications, but only relatively recently has this engine type been expanded to the marine environment. Part of the appeal of this propulsion system is its quick reaction time, reliability, maintainability, and power to weight ratio. To be successful on board a Naval combatant the power output must be high, resulting in an increase in machine size and weight compared to typical aviation applications. In marine applications gas turbine engines are usually coupled in some way to a large set of reduction gears, that not only reduce the high rotational speed of the turbine down to an applicable level for shaft/propeller type propulsion, but they are also firmly fixed in position to reduce damage to the reduction gear due to transmitted vibrations. Typically, these vibrations are considered the result of mass unbalance in the machine's rotating parts, however, the fluid dynamics of the air flow within the engine could produce forces of the same order of magnitude as those forces caused by mass unbalance. As a result, the forced vibrations of these engines must be as low as possible to reduce premature engine failure.

As the Navy expanded the use of these engines, problems developed concerning residual vibrations. All engines delivered to the Navy met specifications for vibration levels, however, some engines were exceeding vibration levels when in operation. Gas generator rotor unbalance was identified as the major cause of higher then normal vibration and premature wear. As a result, the Trim Balancing Technique was developed based on the Least Squares Influence Coefficient method to reduce residual unbalance. The great appeal of this technique is that the whole procedure may be done in place at a fraction of the cost of removal and replacement of the engine. This technique has worked very well and saved the Navy millions of dollars in removal and replacement costs, but it is not 100%

1

effective nor is it permanent. With increasing operational time some engines, previously balanced, show an increase in residual vibration, while others prove incapable of being balanced using this technique [Ref. 1].

The purpose of this Thesis is to examine forces contributing to these vibrations other then simple mass unbalance. Age and increased operating time will induce ware and/or shifting of parts resulting in mass fluctuations, however, it is possible fluid effects of non-uniform flow through the engines rotating parts could produce forces approaching those forces caused by mass unbalance. Some of these rotating parts that could cause non uniform flow are rotating blades, blade tip shrouds, and labyrinth seals. Such forces may even be correctable by current mass balancing techniques if the force and phase of the fluid effects are compatible with the modal shapes selected for balancing.

This thesis will develop a model that predicts the force resulting from the fluid effects induced by a non-circular rotating labyrinth seal. Many of these seals exist in current marine engines, and possess very tight sealing gaps. The mean radius of the seal is usually very large compared to the allowed tolerance. As a result, even a small defect in seal radius compared to the small size of the gap will generate a relatively large effect. Given specific operating flow conditions, forces can be predicted that will rival those allowed by acceptable residual mass unbalance. Given various geometry's and operating conditions it is also possible to predict seal flow regimes.

II.   BACKGROUND

One of the major concerns in rotating machinery design is the residual unbalance due to the mass center of the rotating element not being co-planer with its axis of rotation. Such a situation will result in synchronous lateral vibration on the rotor bearing elements. Under certain situations the magnitude of the lateral displacements caused by this vibration could result in premature failure of the rotor due to fatigue or catastrophic failure of the load bearing elements. Currently mass unbalance is thought to be the major cause of such vibrations, however, bearing wear, non uniform thermal expansion, misalignment between parts, and fluid flow within the machine are other possible causes of lateral vibration. Much work, both analytical and experimental, has been done to detect and reduce these unbalances. In the 1930's dynamically balancing of rotors was widely practiced on test stands with moderate results. As the speed of the machines increased this method proved less effective. Loewy and Piarulli [Ref. 2] point this out and discuss the advantages of modal balancing and self-balancing as effective means of reducing vibrations. Modal balancing works well with the lower modes as long as the harmonic content distribution of the imbalance force is not scattered in the higher modes. Self-balancing makes use of two freely swinging weights within an annular track. As the machine rotates the weights are free to take equilibrium azimuthal positions. At speeds below critical this method tends to add to the unbalance, however, above critical speed the weights reduce the lateral unbalance to zero. Both these methods work for constant speed machines, yet they are not practical for variable speed machines such as those used by the Navy.

For large rotating machinery it is imperative to understand the natural characteristics of each unit, not only to predict critical speeds and safe operating ranges, but also be able to diagnose danger signs in machinery history to avoid catastrophic failure. Muster and

3

Stadelbaur [Ref. 3] discuss the necessity of dynamically balancing a rotor in two or more axial correction planes at one or more operating speeds. Den Hertog [Ref. 4] discuses the technique of shop balancing and then field balancing at rated speed. Some machines at higher critical speeds require multi-planer balancing which does not always result in a balanced rotor. Loewy and Piarulli [Ref. 2] discuss the modal balancing theory that makes use of the natural frequencies and mode shapes of the shaft, which are normally needed for super critical operations. This method works well as long as higher harmonic mode deflection shapes do not resemble the unbalance deflection shape.

With the arrival of the GE LM-2500 Gas Turbine Engine, the United States Navy has become acutely aware of the difficulties of rotor unbalance and the resulting decrease in engine service life. In the late 1970's the SPRUANCE class destroyers and the OLIVER HAZARD PERRY class frigates began fleet operations with a new propulsion plant centered on the LM-2500. Originally this engine had a service life of 5000 hours, yet an alarming rate of engines could not meet this requirement due to high in service residual vibrations. All engines met required vibration levels before delivery, therefore, something was causing an increase in vibrations while these engines were in operation. As a result Thompson, Badgley, and Raczkowski [Ref. 1] developed a trim balancing technique that allows for the balancing of the engine in place at great cost savings. Thompson [Ref. 5] points out that this technique can not always be used effectively. Some engines simply are not capable of being balanced whether due to in service damage, bowed rotor, or some other factor.

One such factor could be fluid forces acting on the rotor due to asymmetries in the rotor airfoils and labyrinth seals rather then simple mass unbalance. The focus of this study will be the potential contribution to synchronous forces from non-circularity in the labyrinth seals and what the magnitude of these forces could be given various design criteria. With the tolerance for a seal radius being a few thousandths of an inch on a disk

4

with a radius of one to two feet and a nominal gap clearance on the order of thousandths of an inch, there exists a possibility for substantial gap variation. It is the mean gap clearance along with the radius tolerance that produces the gap variation.

A labyrinth seal is not a seal at all. Given a proper rotor/stator configuration, there is no contact between the rotating labyrinth knives and the stationary casing. The propose of the labyrinth is to create a path for the fluid to travel that causes a substantial change in kinetic energy within the seal gland area. This change in kinetic energy, which dissipates in successive chambers, creates areas of pressure variation upstream of the gland compared to the exit pressure of the gland, which seals the upstream from the downstream conditions.

A perfect operating seal with no intolerance in the seal gaps has uniform pressure and flow momentum changes within the seal gland area. There is no resultant radial force on the shaft. If some non circular intolerance did exist on the seal knife, then the flow through the seal would not be uniform, causing areas of higher mass flow. The ultimate result is a non uniform pressure distribution. If a non uniform pressure distribution exists in the gland, it is a simple calculation to convert it to a radial force in magnitude and phase relative to the rotating reference system.

Gas turbine rotors are typically balanced to G2.5 limits as specified by ISO 1940 [Ref. 6]. Given these constraints the goal is to maintain the residual mass unbalance force to less than 1 N for every Kg of rotor mass at 10,000 RPM. This mass unbalance force is described as $F = m_e r_e \omega^2$, where $m_e r_e$ is the equivalent unbalance (kg-m) and ω is the shaft rotational speed (rad/sec). Once the fluid force is known it is compared to that of the mass unbalance force. A comparison gives some indication of the significance such fluid forces could have on rotor unbalance and the possible necessity to consider them in the design process. Under certain conditions these forces may present no significant obstacle to the modal balancing techniques currently used. If the force is of significant magnitude or

5

phase to impact on specific mode shapes, correction by simple adjustment of the mass distribution may not be possible, which is precisely the condition experienced in some LM-2500's (Thompson [Ref. 5]).

III. MODEL FORMULATION

A.   FLOW EQUATIONS

The flow in a labyrinth seal is three dimensional, turbulent, highly unsteady, and compressible. Since the effects of this complicated flow, not the details, are of direct interest for this problem, a simplified lumped parameter fluid model, used by Kostyuk [Ref. 7], Iwatsubo [Ref. 8], and Millsaps [Ref. 9], will be introduced. This model treats the flow in the labyrinth chamber as a one-dimensional flow in the azimuthal direction, but allows for axial influx and efflux due to the pressure driven flow through the seal gaps. This type of model contains the dominant physics that generate a non-uniform pressure distribution in the azimuthal direction within the gland. The mechanism driving this pressure distribution is non-uniform mass and azimuthal momentum exchange between the upstream receiver and the seal gland. Along with the basic model simplifications, several other simplifications are made

1. Ideal gas. Pv=RT
2. Adiabatic Process
3. The axial flow is calculated using a Bernoulli equation based on the local pressure difference at a given time and angular location using the average density.
4. The frictional shear stress on the fluid in the azimuthal direction within the gland can be calculated using the Darcy friction law for 1-D flow.
5. No duct acoustic resonance occur in the range of interest.

It is also assumed that the seal is fed by a uniform upstream plenum. This condition is not strictly met, however, the perturbation flow will induce a flow redistribution in the upstream volume, helping to simplify the analysis. Care must be exercised, however, since under certain conditions the non uniformity in the upstream flow can have a strong

7

impact on the flow in the seal. In particular, a large force augmentation is possible as a result of the upstream non-uniformity. An analysis of this phenomena for a whirling seal with a finite upstream volume is given by Millsaps and Martinez [Ref. 10].

The one-dimensional continuity equation for the flow along the azimuth inside the seal gland may be written as

$$\frac{\partial}{\partial t}[\rho A] + \frac{1}{R_s}\frac{\partial}{\partial \theta}[\rho A V] + q_2 - q_1 = 0 \tag{1}$$

where the first two terms are the normal 1-D continuity relation for a deformable duct. The fluid density is ρ, V is the swirl velocity in the gland, and A the gland cross sectional area normal to V. The remaining terms are due to the axial mass flux over the outlet and inlet knives respectively.

The one-dimensional momentum equation, which includes the rotor and stator frictional shear stresses, τ_s and τ_r , is similarly written as,

$$\frac{\partial}{\partial t}[\rho A V] + \frac{1}{R_s}\frac{\partial}{\partial \theta}\left[\rho A V^2\right] + q_2 V - q_1 V_i + \tau_s l - \tau_r (l + 2h) + \frac{A}{R_s}\frac{\partial P}{\partial \theta} = 0 \tag{2}$$

The inlet swirl is given by V_i , and the last term is the induced pressure gradient force. The total incoming mass flow is $\dot{m} = \rho A_s w$ where A_s is the effective circumferential gap area and w is the jet axial velocity. The effective inlet area seen by the flow is the real flow area multiplied by a flow coefficient (μ). The first knife coefficient will typically be $\mu_1 = .65$. The resulting mass influx per unit circumferential length (q_1) is therefore,

$$q_1 = \mu_1 \rho_1 \delta_1 V_1 \tag{3}$$

A similar equation applies for the mass efflux per unit circumferential length, however, the flow coefficient may be somewhat higher due to the kinetic energy carry over effect.

To calculate the inflow (q_1) Bernoulli's equation is used with the density being averaged between the upstream and seal gland. This yields,

$$q_1 = \frac{\mu_1 \delta_1}{\sqrt{R_a T}} \left(P_i^2 - P^2 \right)^{\frac{1}{2}}$$
(4)

where P, δ_1 and q_1 are functions of time and angle. Similarly, for the outlet flow

$$q_2 = \frac{\mu_2 \delta_2}{\sqrt{R_a T}} \left(P^2 - P_o^2 \right)^{\frac{1}{2}}$$
(5)

The shear forces in the gland from both rotor and stator, which are responsible for changing the average swirl of the fluid in the gland, are calculated by using the Darcy friction coefficients law

$$\tau_s = \frac{\rho}{8} \lambda_s sgn(V) l V^2 \quad \text{and} \quad \tau_r = \frac{\rho}{8} \lambda_r sgn(\omega R_s - V)(2h + l)(V - \omega R_s)^2$$
(6)

The friction coefficients, λ_s and λ_r, are calculated using Blausius' formula with the relevant local Reynolds number, based on the gland hydraulic diameter and the relative tangential velocity between the solid surface in question and the mean swirl velocity within the gland

$$\lambda_{s,r} = 0.3164 \Re^{(-0.25)}$$
(7)

9

These equations will be used to determine the circumferential flow inside a spinning seal that does not have perfect circularity.

B.   SEAL IMPERFECTION

A labyrinth seal is nominally circular unless there are small deviations, which could be due to machining tolerances as well as in service degradation. A very small "waviness" in the height of the seal knives can introduce substantial relative variations in flow area, especially at operating conditions where seal clearances are the tightest.

Letting the circumferentially averaged gap for the first knife be denoted by δ_1^*, and the local gap be $\delta_1(\theta)$, where θ is the angular coordinate, the resulting difference (error) is e_1. The local gap for a stationary seal can be expressed as

$$\delta_1(\theta) = \delta_1^* + e_1(\theta) \tag{8}$$

The net radial force on the rotor due to a pressure distribution around the seal gland is

$$F_r = -\pi l \int_{-\pi}^{\pi} P(\theta)e^{i\theta}d\theta \tag{9}$$

From orthogonality, only the first harmonic component of $P(\theta)$ will contribute to the radial force. Since the perturbation analysis to follow is purely linear, it is sufficient to retain the first harmonic of the seal geometric imperfection to obtain the first harmonic in pressure perturbation. The first harmonic of the axial flow area is given by

$$\hat{\varepsilon} = \frac{1}{\pi} \int_{-\pi}^{\pi} \delta(\theta)\cos(\theta)d\theta \tag{10}$$

For convenience, the extra flow area can be concentrated at a single location and would appear as a notch. Mathematically this can be treated as a Dirac delta function. Alternatively, this imperfection is equivalent to a circular seal whose center is displace a distance e from the center of rotation and land centroid. Figure 1 shows a typical non-uniform sealing gap for a single knife, along with the equivalent first harmonic and notch representations. Figure 2 shows the 2-D geometry of a single gland seal with a notch imperfection modeled as a single notch. Figure 3 shows both the first and second knives in a 3-D representation, with the first knife imperfection being at a different location as the second knife imperfection. When spinning, the first knife non-dimensional gap distribution is given by

$$\frac{\delta_1(\theta,t)}{\delta_1^*} = 1 + \hat{\varepsilon}_1 e^{i(\theta - \omega t)} \tag{11}$$

Where $\hat{\varepsilon}_1$ is the amplitude of the first harmonic deviation from circularity. Similarly, for the second knife the imperfection is represented by

$$\frac{\delta_2(\theta,t)}{\delta_2^*} = 1 + \hat{\varepsilon}_2 e^{i(\theta - \omega t)} \tag{12}$$

Finally, a representation for the seal gland not having the same center as the casing is made. The height of the gland is given by

$$\frac{h}{h^*} = 1 + \hat{\varepsilon}_3 e^{i(\theta - \omega t)} \tag{13}$$

11

Note that $\hat{\varepsilon}_1$, $\hat{\varepsilon}_2$ and $\hat{\varepsilon}_3$ are in general complex so that they contain phase information on the location of the imperfections as well as the amplitude of the imperfection. A perfect casing will be considered here. A first harmonic deviation in the land would produce a steady force on the rotor in the absolute frame. Since the magnitude of this force would be small compared to the weight of the rotor, it is probably of little importance and will not be considered in this model.

The imperfection generating the forces does not have to be due to sealing gap area variations. Flow coefficient asymmetries due to tip imperfections can also generate mass flow perturbations and hence radial forces. For the purposes of this model, only forces generated from seal gap non-circularity will be considered.

C.   SOLUTION TECHNIQUE

An approximate solution for the azimuthal pressure in the seal will be found by a linear perturbation analysis. The zeroth order solutions for the case of a perfect seal, which are independent of time and angle, are found from Equations (1) and (2) by noting $\partial[] / \partial t = 0$ and $\partial[] / \partial \theta = 0$. All zeroth order solutions will be denoted with $[]^*$. The steady pressure, density and flow rate are extracted from the zeroth order solution to Equation (1)

$$P^* = \left[\frac{\mu_1^{*2}\delta_1^{*2}P_i^2 - \mu_2^{*2}\delta_2^{*2}P_o^2}{\mu_1^{*2}\delta_1^{*2} + \mu_2^{*2}\delta_2^{*2}} \right]^{\frac{1}{2}} \tag{14}$$

$$\rho^* = \frac{P}{R_a T} \tag{15}$$

$$q^* = \frac{\mu_1 \delta_1}{\sqrt{R_a T}}\left(P_i^2 - P^{*2} \right)^{\frac{1}{2}} \tag{16}$$

12

Equation (2) is used to solve for the zeroth order swirl velocity (V^*). For fixed friction factors the resulting equation is of a quadratic form in V^*. Since the friction factors are functions of V^*, in that they are a function of the local Reynolds number, the following quadratic equation in V^* must be solved by iteration. The inlet swirl velocity (V_i) is used as an initial guess

$$\frac{\rho^*}{8}[\lambda_s l - \lambda_r(l+2h)]V^{*2} + \left[q^* + \frac{\rho^*\lambda_r}{4}(1+2h)\omega R_s\right]V^* - \left[q^*V_i + \frac{\rho^*\lambda_r}{8}(1+2h)\omega^2 R_s^2\right] = 0 \qquad (17)$$

With the flow conditions for the problem of the perfect rotor obtained, a perturbation solution for the imperfect rotor will be sought. Since it is assumed that the pressure and velocity inside the gland can be represented as the zeroth order values plus small perturbations, which are functions of (t,θ), they may be represented as

$$P = P^*\left[1 + \xi(\theta,t)\right]$$
$$V = V^*\left[1 + \eta(\theta,t)\right] \qquad (18)$$

The first harmonics of these being functions of time and angle can be expressed as

$$\xi = \hat{\xi}\, e^{i\,(\theta-\omega t)} \qquad (19)$$

$$\eta = \hat{\eta}\, e^{i\,(\theta-\omega t)} \qquad (20)$$

When these expressions are substituted into Equation (1) and linearized, the continuity equation becomes

13

$$\left\{ q^* \left[\frac{P^{*2}}{P_i^2 - P^{*2}} + \frac{P^{*2}}{P^{*2} - P_o^2} \right] + \frac{\rho^* lh^*}{\gamma} \left(\frac{V^*}{R_s} - \omega \right) i \right\} \hat{\xi} + \left\{ \frac{\rho^* lh^* V^*}{R_s} i \right\} \hat{\eta}$$

$$= \left\{ q^* \right\} \hat{\varepsilon}_1 + \left\{ -q^* \right\} \hat{\varepsilon}_2 + \left\{ \rho^* lh^* \left(\omega - \frac{V^*}{R_s} \right) i \right\} \hat{\varepsilon}_3 \qquad (21)$$

Similarly, the linearized momentum equation, Equation (2), becomes

$$\left\{ q^* \left[\frac{P^{*2} V^*}{P^{*2} - P_o^2} + \frac{P^{*2} V_i}{P_i^2 - P^{*2}} \right] + \left(\frac{\rho^*}{8\gamma} \right) \left(\lambda_s l V^{*2} - \lambda_r (l + 2h^*)(\omega R_s - V^*)^2 \right) + \left[\frac{\rho^* V^* lh}{\gamma} \left(\frac{V^*}{R_s} - \omega \right) + \frac{P^* lh^*}{R_s} \right] i \right\} \hat{\xi}$$

$$+ \left\{ q^* V^* + \frac{\rho^* V^*}{4} \left(\lambda_s l V^* - \lambda_r (l + 2h^*)(V^* - \omega R_s) \right) + \rho^* V^* lh^* \left(\frac{2V^*}{R_s} - \omega \right) i \right\} \hat{\eta}$$

$$= \left\{ q^* V_i \right\} \hat{\varepsilon}_1 + \left\{ -q^* V^* \right\} \hat{\varepsilon}_2 + \left\{ \rho^* lh^* V^* \left(\omega - \frac{V^*}{R_s} \right) i \right\} \hat{\varepsilon}_3 \qquad (22)$$

Equations (21) and (22) are a set of linear complex algebraic equations, easily solved to yield the complex amplitudes of the pressure and velocity perturbations. The pressure amplitude is given in terms of the real and imaginary parts, $\xi_\Re$ and ξ_3, respectively as

$$\hat{\xi} = \xi_\Re + i \xi_3 \qquad (23)$$

The amplitude of the pressure perturbations is

$$|\hat{\xi}| = \sqrt{\xi_\Re^2 + \xi_3^2} \qquad (24)$$

14

and the phase relative to the reference imperfection is

$$\psi_\xi = \tan^{-1}\left(\frac{\xi_\Im}{\xi_\Re}\right) \tag{25}$$

To calculate the force on a rotor due to the non-uniform pressure distribution, which is now represented by the amplitude of the pressure perturbation, it is now a simple task of converting this pressure to force. This magnitude is all that is sought in this analysis, however, it should be noted that phase information can also be extracted, which may prove important in modal vibration analysis and balancing.

VI. MODEL PREDICTION

A.   SEAL FLOW CONDITIONS

The solutions to Equations (21) and (22) depend on the zeroth order parameters. These conditions depend on nominal seal geometry, inlet flow conditions (P_i and V_i), and speed of the rotor. Figure 4, which shows solutions to Equation (17) based on a wide variation in nominal seal geometry, inlet flow conditions (P_i and V_i), and speed of the rotor, provides non dimensional interrelationships among these parameters for a fixed seal geometry typical of modern gas turbines (namely the sealing height and pitch being equal). Figure 4 is a map that indicates what flow "regime" occurs for a given set of conditions. For example, if the axial flow rate through the seal is small and the difference between the peripheral speed of the rotor (ωR_s) and the inlet swirl velocity (V_i) is large, then the fractional change in swirl will be large. On the other hand, if the flow rate is large, due to a large pressure gradient or large sealing gaps, and the wheel speed is about the same as the inlet swirl, there will be a relatively small fractional swirl change. If E is about 1.5, there is little tendency for the swirl to change, as would be expected, since this is the "equilibrium" swirl value that would be obtained in the absence of an axial through flow.

B.   RADIAL FORCE PREDICTIONS

Results for particular cases will now be presented to illustrate the use of this model in the prediction of synchronous radial rotor forces. Table 1 shows the seal geometry used. The seal's operating conditions and geometry are typical for an LM-2500 gas generator. The dominant parameters controlling the forces are:

1. The pressure difference across the seal knives.
2. The inlet swirl velocity.
3. The swirl change through the seal.
4. The magnitude of the seal imperfection relative to the nominal gap.
5. The angle of the second seal imperfection relative to the first.

The general scaling behavior for the radial synchronous force is approximately proportional to the inlet total to exit static pressure difference ($P_i - P_o$) as would be expected for incompressible flow. Some nominal deviation from this scaling occurs at higher pressure ratios due to compressibility effects. Due to the linearity of the model, the predicted forces will scale directly with the magnitude of the imperfection used for the seal. When the magnitude of the seal non-circularity doubles for a given nominal seal gap, the force doubles accordingly. Similarly, for a fixed non-uniformity, the force scales inversely with the nominal seal gap. With the force scalings proportional to the geometry, it will be possible to non-dimensionalize and present the force as

$$\tilde{F} = \frac{F}{\Delta P l R_s \varepsilon_1} = \frac{F \delta_1^*}{\Delta P l R_s e_1} \tag{26}$$

1.   Single Knife Imperfection

The magnitude of the radial force due to an imperfection in the first sealing knife is shown in Figure 5. The force coefficient is shown verses rotational frequency for several values of inlet swirl velocities. As the inlet swirl increases, the frequency at which the minimum force occurs also increases. To obtain a better understanding of the phenomenon taking place, Figure 6 is shown with the exact conditions as those for Figure 5, except the effects of friction are taken out of the model. With no friction there is no mechanism for changing the swirl of the incoming flow and as a result the minimum force

occurs when the rotational speed of the rotor equals the swirl speed in the gland. This suggests that the minimum force occurs when the rotor speed is equal to the swirl speed in the gland. Returning to Figure 5, the effects of friction are not only impacting on the swirl speed in the gland, but the momentum change of the flow absorbs some of the energy from the force that could have been imparted to the rotor. At the minimum force condition the gland swirl speed is the same as the rotor speed, meaning there is no relative motion between them. The friction within the gland always changes the speed of the incoming swirl depending on the relative velocity between the inlet swirl and the rotor speed. Figure 7 shows the phase or relative position where the force acts on the rotor. The phase shift corresponds to that frequency where the force is a minimum. The phase is a function of rotor speed.

2.   Duel Knife Imperfection

In this case the same conditions exist as in Table 1, however, both the front knife and the rear knife are capable of having a non-circularity. These non circularities are also capable of having a phase angle between them, which may very from 0 to 180 degrees. Figure 8 shows the effect of the phase angle of the back knife notch relative to the front notch as a function of rotor speed. The size of each imperfection is the same, and the inlet swirl is maintained at 150 m/s. Results are shown for the angle between the imperfections varying from 0 to 180 degrees. The force tends to be less when the notches are at the same location. This is due to a local increase in pressure at the front seal imperfection being partially negated by a local decrease in pressure at the rear seal imperfection. It should also be noted that the maximum force occurs when the rotor speed equals the speed of the gland swirl, which is not consistent with the trend of having a minimum force at this point. This case can be described as a bowed rotor. Even though the pressure effects tend to cancel they are still significant. When the imperfections are not

18

lined up the forces are larger implying the pressure effects of the front and back imperfections are additive.

C.   MULTIPLE SEALS

Up to this point, the forces from single gland labyrinth seals have been considered. The analysis that has been presented can be readily extended to the case where there are multiple sealing knives within a single labyrinth seal. The results for multi-cavity seals show similar trends to those of a single gland seal. For a single gland labyrinth seal it has been shown that two complex algebraic equations will predict the fluid forces within the gland. This analysis can be easily expanded for N number of chambers within a multi-chamber labyrinth seal. The extension of this analysis will yield 2-N equations with 2-N unknowns. This is not treated explicitly here.

Typically, a gas turbine possesses dozens of locations in the secondary flow path where labyrinth seals are placed. In this case there are multiple seal glands which are not coupled along the flow path. It is important for a designer to be able to incorporate the radial forces arising from imperfect seals at different axial locations. The question that arises is: How does one "add" the forces? Two special cases will now be discussed.

1.   In Phase

If the imperfections of all the rotor seals have the same angular location then the forces are added. This would be the case if the rotor were slightly bowed, or if the seals were all machined together with a slight off-set on the lathe. The result being that all the forces would occur at the same location. This can be expressed as

$$F_T = \sum_{i=1}^{N} F_i = NF \qquad (27)$$

Where F_T is the total radial force, F_i is the force from the ith seal and N is the number of seals. Using the conditions of Table 1 and assuming 16 stages with a uniform non-circularity of 1, the model predicts the resulting force will be 515 N. A non-circularity of one is very high for a modern gas turbine, but given the tight tolerances it is not impossible. A non-circularity of .1 is quite possible under normal operating conditions and would yield a force of 51.5 N on the rotor.

2. Random Phase

If the imperfections are random, then there is no phase correlation between the imperfection at one location and any other location. It may appear in this case that the forces may totally cancel but, this is analogous to the case of a random walk. It can be shown that the most probable magnitude of such an addition of forces with random phases would scale with the square root of the number of seals.

$$F_T = F\sqrt{N} \tag{28}$$

Given the same conditions as the "bowed rotor" case, the model predicts the force on the rotor for a non-circularity of 1.0 will be 128 N. Similarly, if the non-circularity were .1 the force on the rotor would be 12.8 N. It is expected that the net radial force will be somewhere between these limits of completely in phase and totally random.

D.   FLUID FORCE COMPARED TO UNBALANCE FORCE

The fluid force must be of the same order of magnitude as the force due to the residual mass unbalance if it is to be considered important in the dynamics of the rotor. From ISO 1940 [Ref. 6] the acceptable radial force which corresponds to a G2.5 balancing grade is roughly 0.1 Newtons per kilogram of rotor mass at 1000 RPM and about 1.0 Newtons per kilogram at 10,000 RPM.

Since the LM-2500 engine has been used to model the geometry used, it is appropriate to use the mass of the rotor to make comparisons. The mass of the rotor is about 500 kilograms. The normal operating speed or the rotor is about 10,000 RPM. With these conditions the limiting mass unbalance is 1.0 Newtons per kilogram. In the cases previously discussed the forces predicted convert to mass unbalance forces of 1.03 - .3 Newtons per kilogram for a non-circularity of 1, and 0.1 - 0.03 Newtons per kilogram for a non-circularity of 0.1. These predicted unbalance forces are on the same order of magnitude as the limiting mass unbalance force.

TABLE 1. STANDARD CASE CONDITIONS

DIMENSIONS	ATMOSPHERICS
Rs = .5 m	Pi = 110000 Pa
L = .01 m	Po = 100000 Pa
h = .01 m	T = 295 K
δ_1 = .0001 m	
δ_2 = .0001 m	
ω = 1000 rad/sec	

21

V. CONCLUSIONS

A lumped parameter fluid model was presented that predicts the generation of synchronous radial forces due to a rotating imperfect labyrinth seal. The predictions may be based on knife imperfections for the front knife, the back knife, or both with any angle between them. The model is capable of predicting the magnitude of the resulting force and the angular location on the rotor. The flow characteristics produced by the model are consistent with those expected, in that, the non-dimensional flow regimes are consistent with physical behavior.

The forces predicted by this model are of the same order of magnitude as those recommended for some common balancing grades. The phase predicted could also have an impact on the modal balancing techniques currently used, since the phase of these forces is a function of rotor speed not rotor mass. This behavior must be incorporated into the trim balancing technique if the balancing masses are to account for the residual fluid forces.

The model predicts that a minimum force condition is always consistent with a rotor speed that matches the gland swirl speed. This implies a design criterion calling for an inlet swirl speed that matches rotor speed. Such a condition will reduce residual fluid forces imparted to the rotor. Currently swirl breaks are used in engine design to reduce inlet swirl and help reduce rotor instability. It is possible that while swirl breaks help solve the rotor instability problem, they may add to the synchronous, forced vibration problem. This condition is not yet manifesting itself since rotor mass is still relatively high. With increasing advances in materials and rotor bearing design, rotor mass will decrease while machine power density increases. At some point the fluid forces produced by component non circularity could become more significant than the mass unbalance forces. Under such conditions it may not be possible to balance these forces with mass corrections, meaning

proper design and the ability to predict such fluid forces based on given tolerances will be imperative to rotor balance.

VI. RECOMMENDATIONS

Many simplifying assumptions have been made in order to reduce this highly complex flow pattern down to a model that could make some predictions consistent with the dominant physics taking place within the gland. The results are promising, however, they must be verified with experimental data. It is recommended that a test facility be constructed so that the conditions described here may be reproduced on a test platform. It is anticipated that discrepancies will arise, however, if scaling factors can be applied to make the model accurate then it will be possible to predict what design tolerances will produce in the way of fluid forces on the rotor.

The phase component of the force produced was briefly touched on in this study, yet it may prove to have a profound effect on current balancing techniques, since the phase of this force is a function of rotor speed not rotor mass. It is recommended that this be studied further.

On the modern gas turbine engine, labyrinth seals are not the only source of fluid induces synchronous forces. Each rotating blade tip is structured to act as a seal in order to reduce leakage, hence increasing component efficiencies. Any non circularity in blade tip radius will cause non uniform radial clearances resulting in non uniform radial forces. As this model has shown, blade to blade variation in radial forces could affect rotor balance. These radial forces at the blade tips should be studied for possible contributions to synchronous force vibrations and the balancing problem.
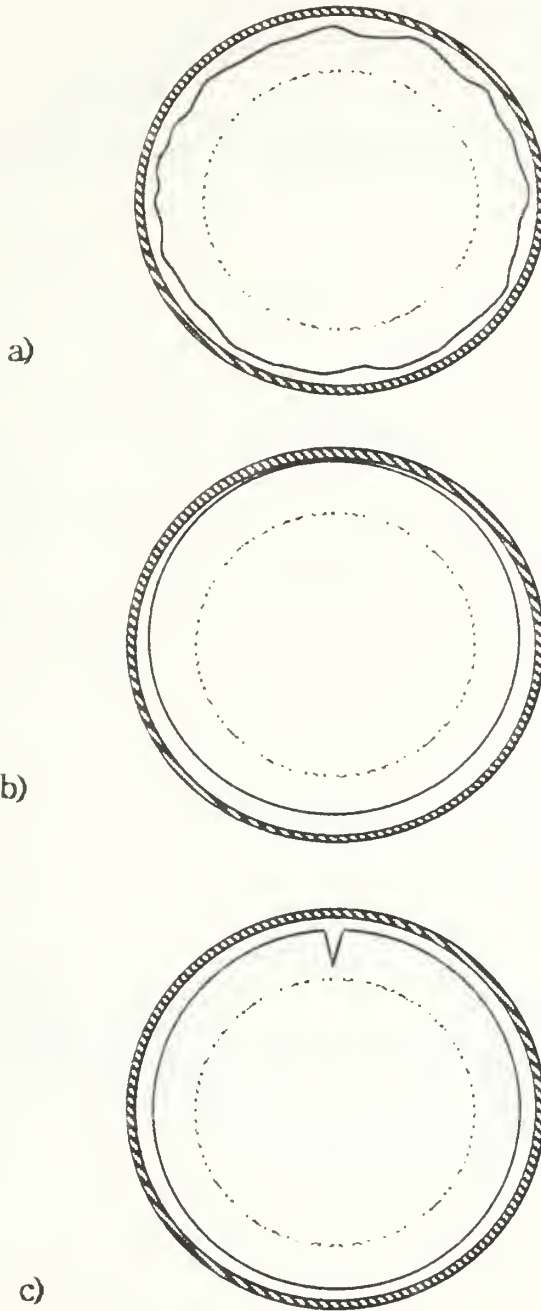
Figure 1. Three equivalent sealing gap representations for a non-uniform
          single labyrinth knife: a) Exaggerated non-uniformity,
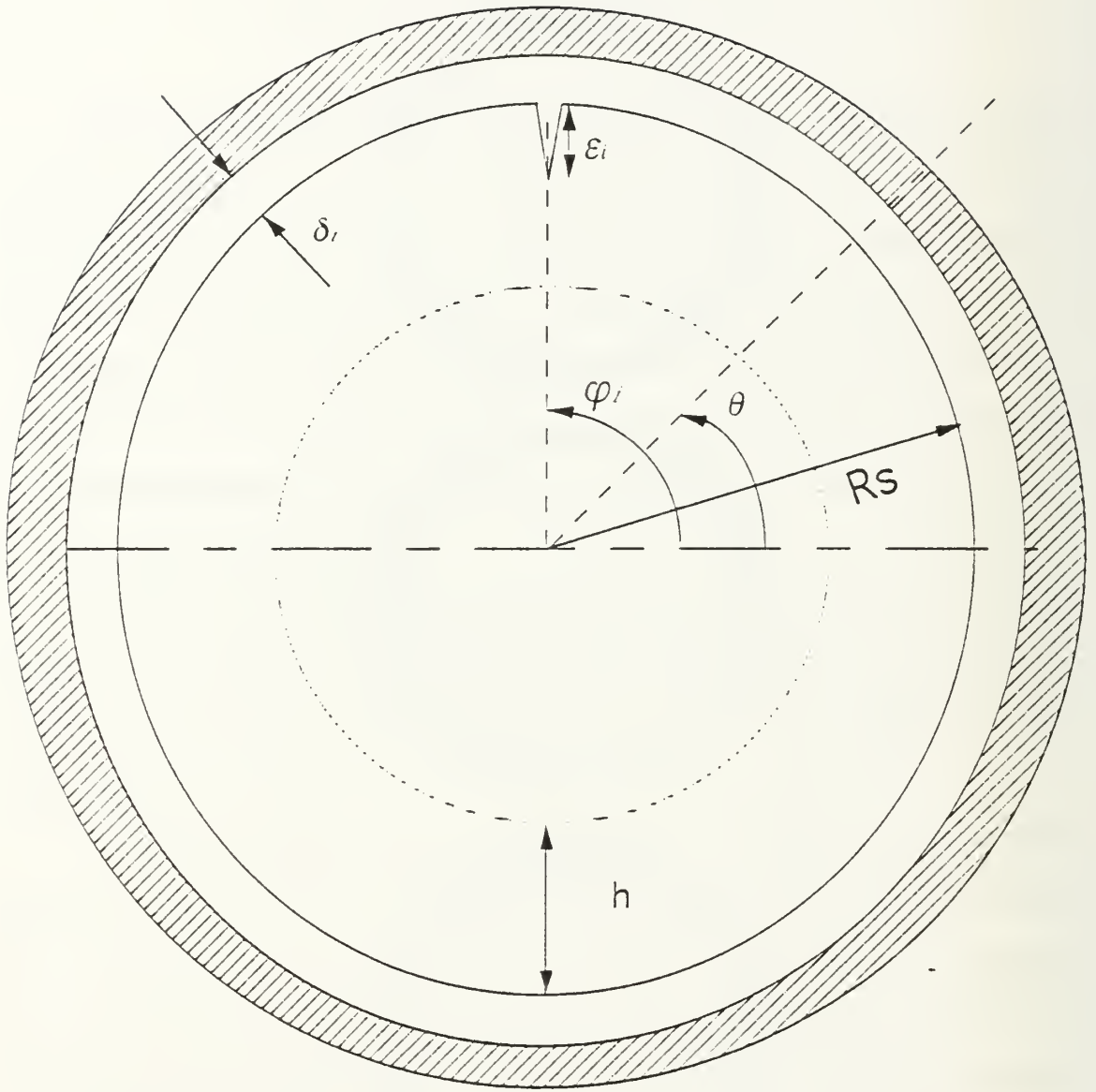   b) Equivalent first harmonic, c) Equivalent notch

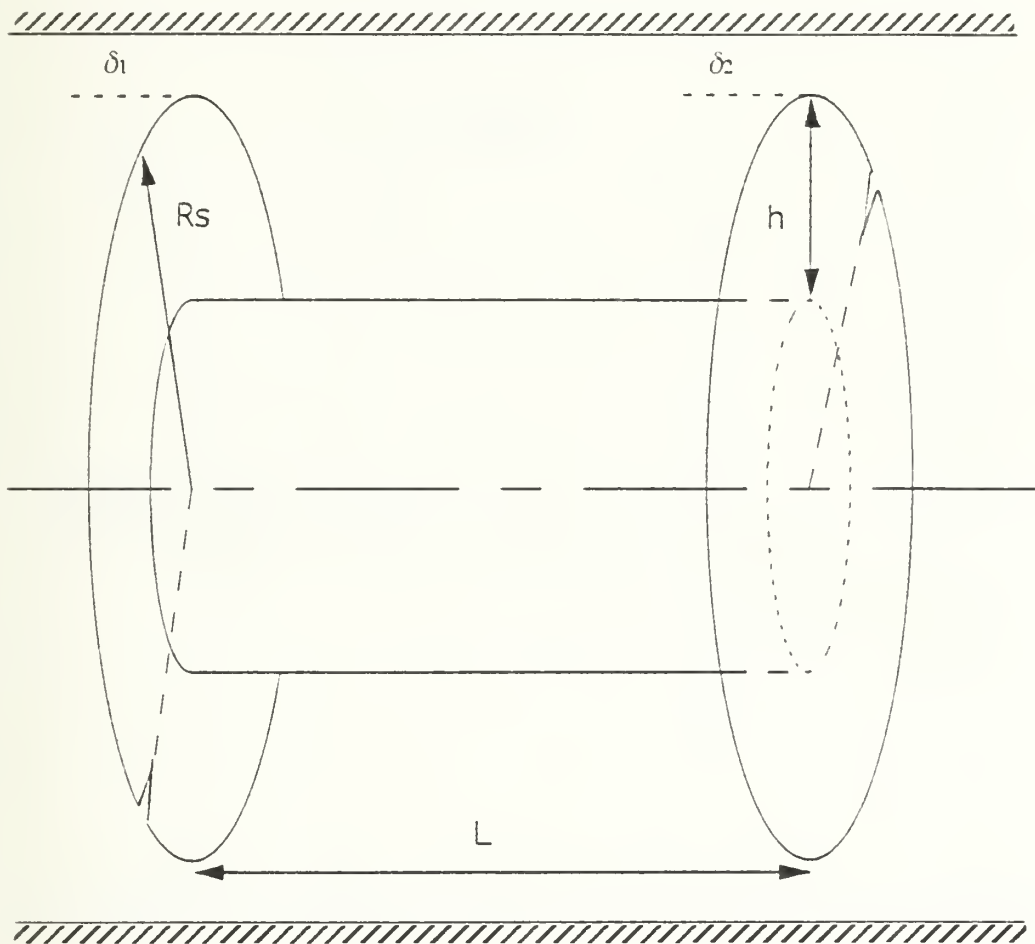Figure 2. Two dimensional view of notch reference frame for single knife

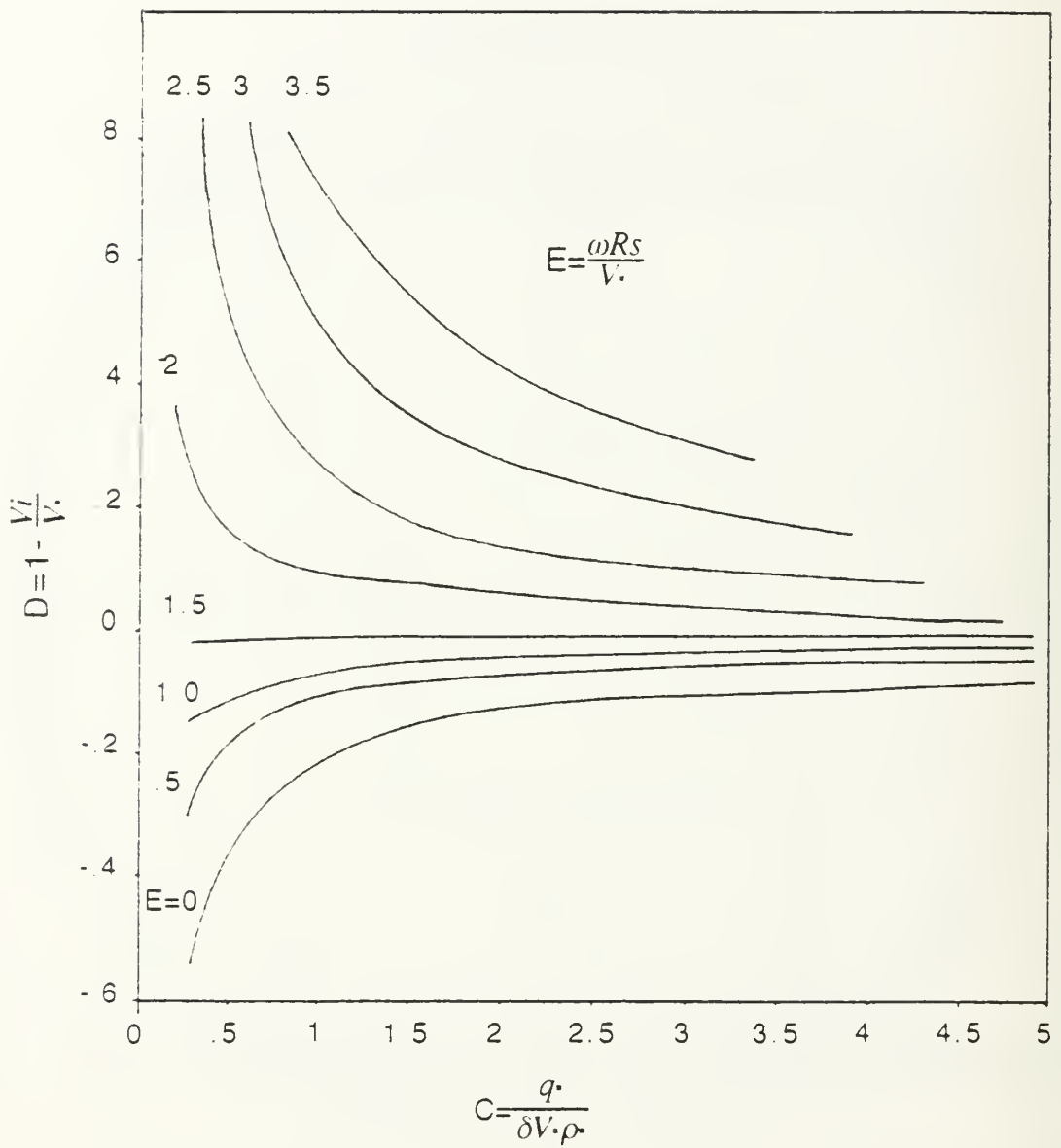Figure 3. Three dimensional view of two knife labyrinth seal

Figure 4. Plot for nondimensional interrelationship for seal through flow (C), shaft spinning speed (E), and swirl change (D) in the labyrinth gland.
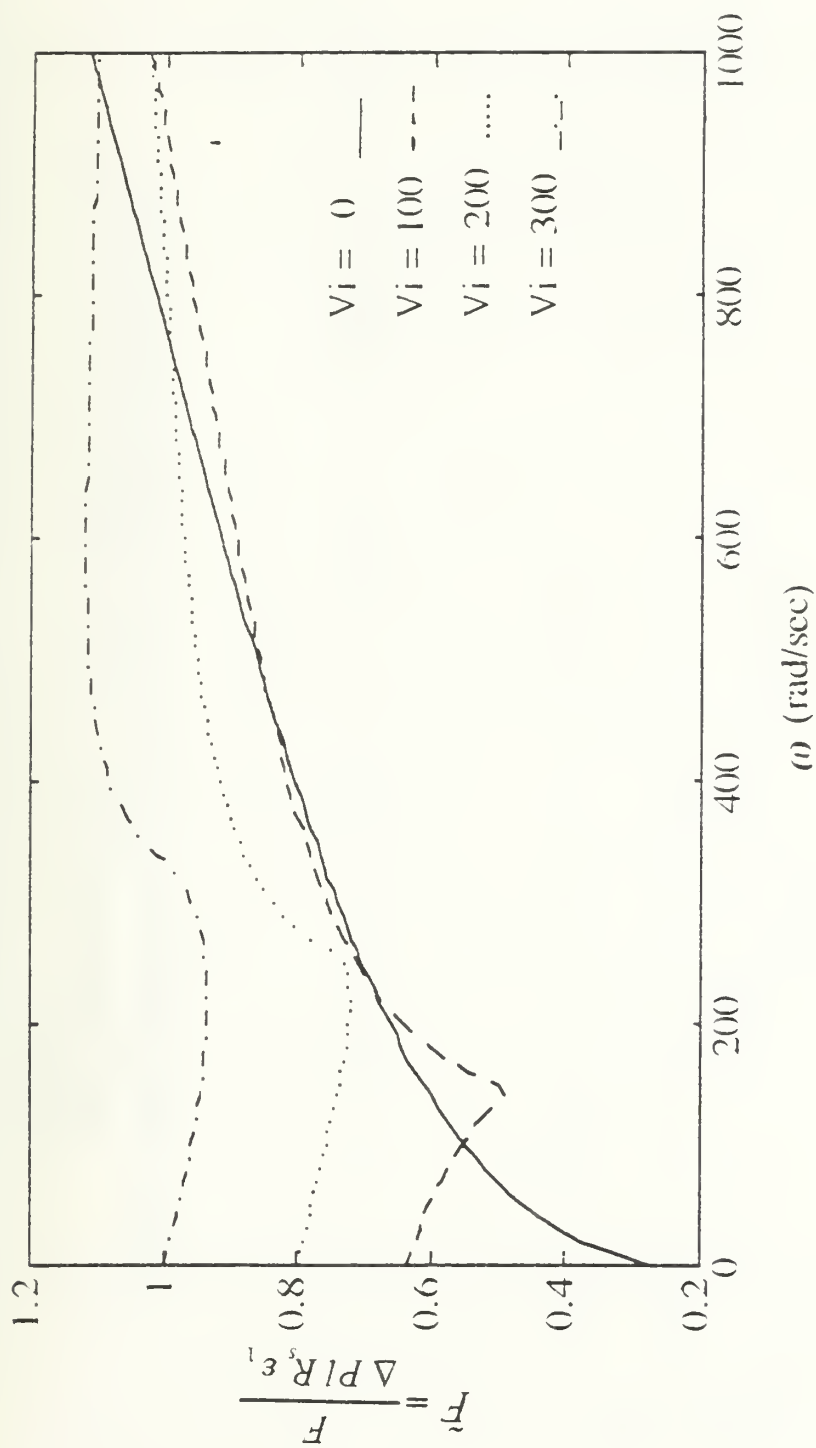
Figure 5. Force coefficient for a seal with a front knife imperfection versus rotor angular frequency using inlet swirl as a free parameter as predicted by the model.
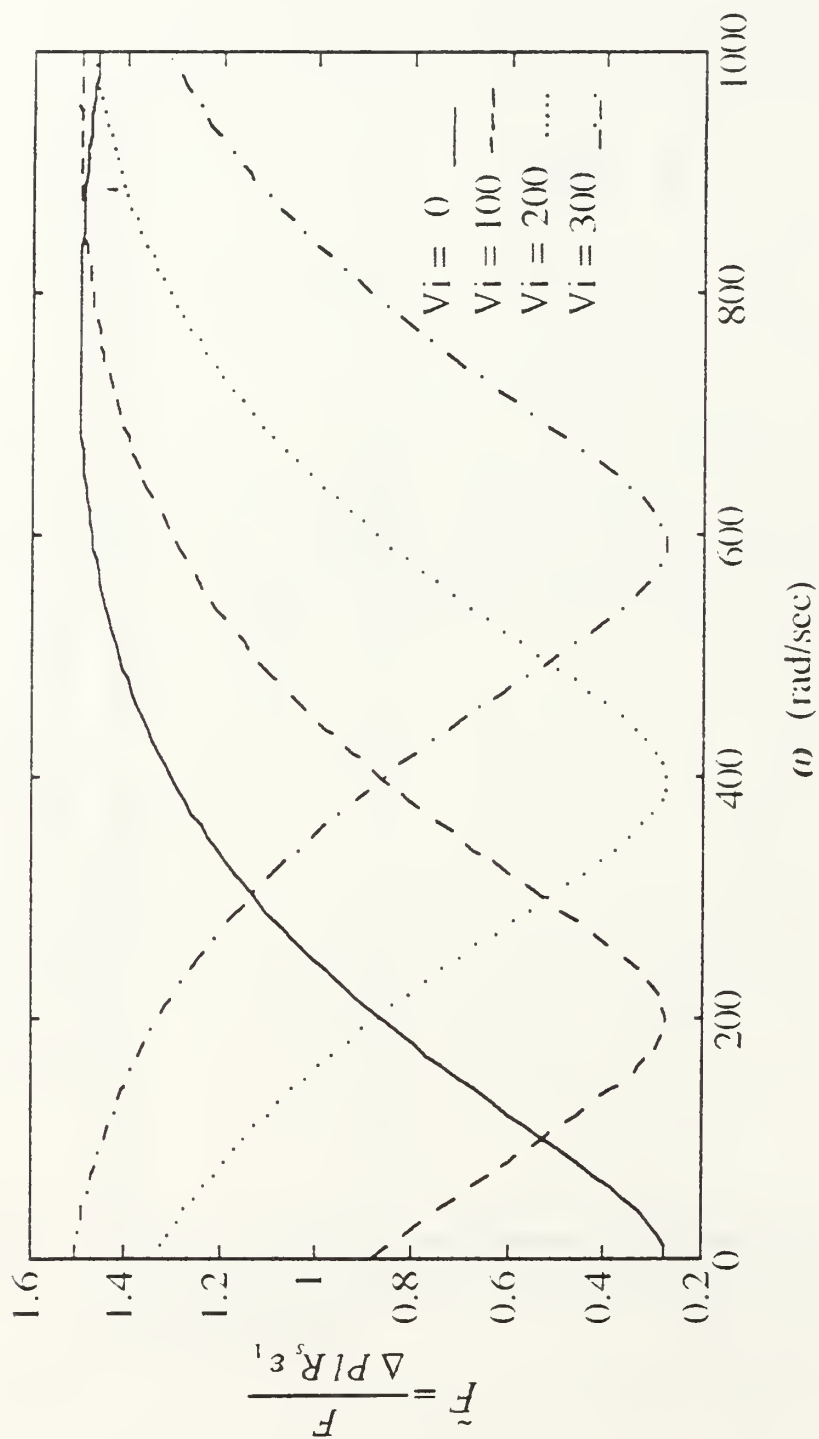
29

Figure 6. Force coefficient versus rotor angular frequency with frictional shear stresses neglected. All other conditions are the same as in Figure 5.
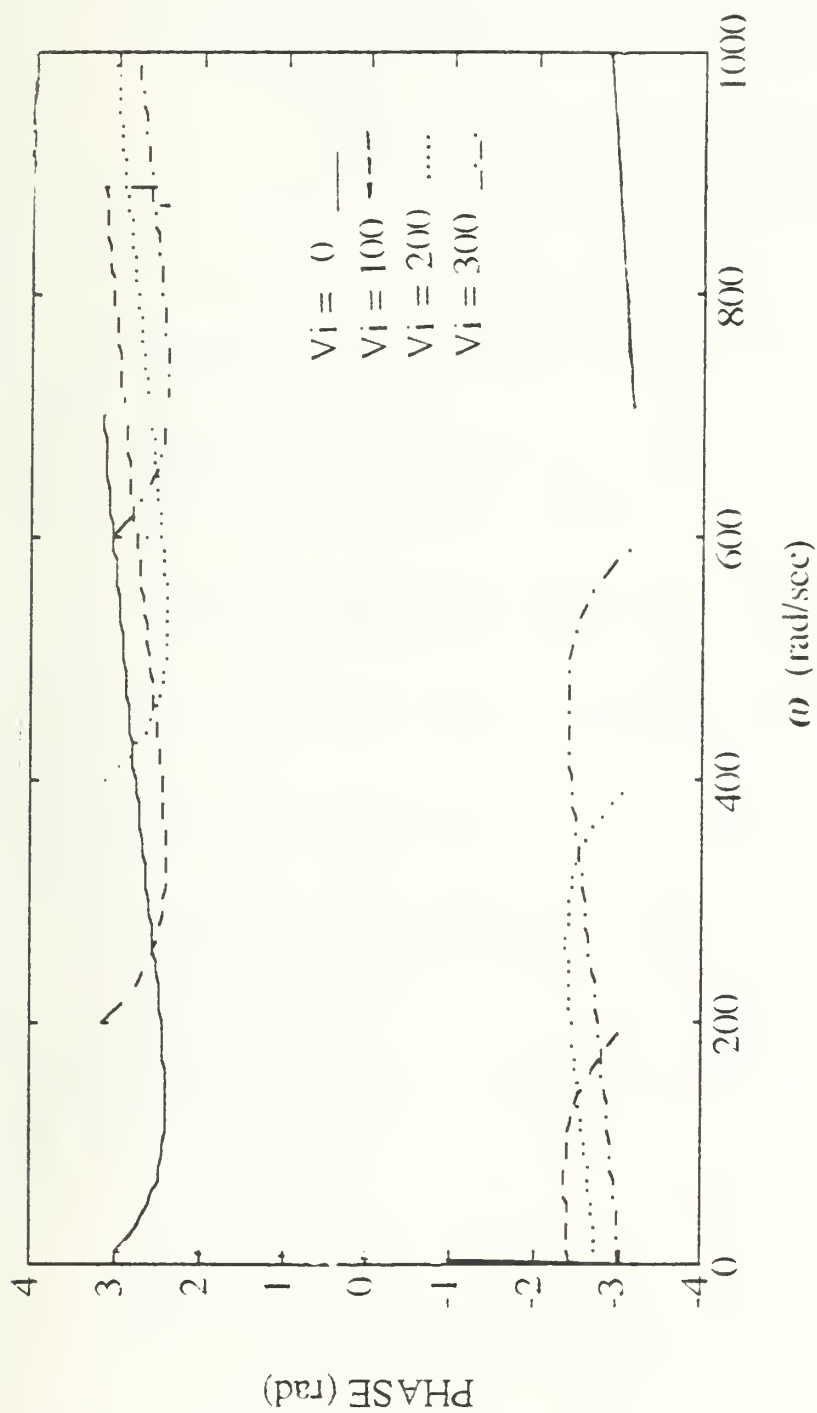
30

Figure 7. Phase of the force on the rotor relative to the notch versus rotor spin speed.
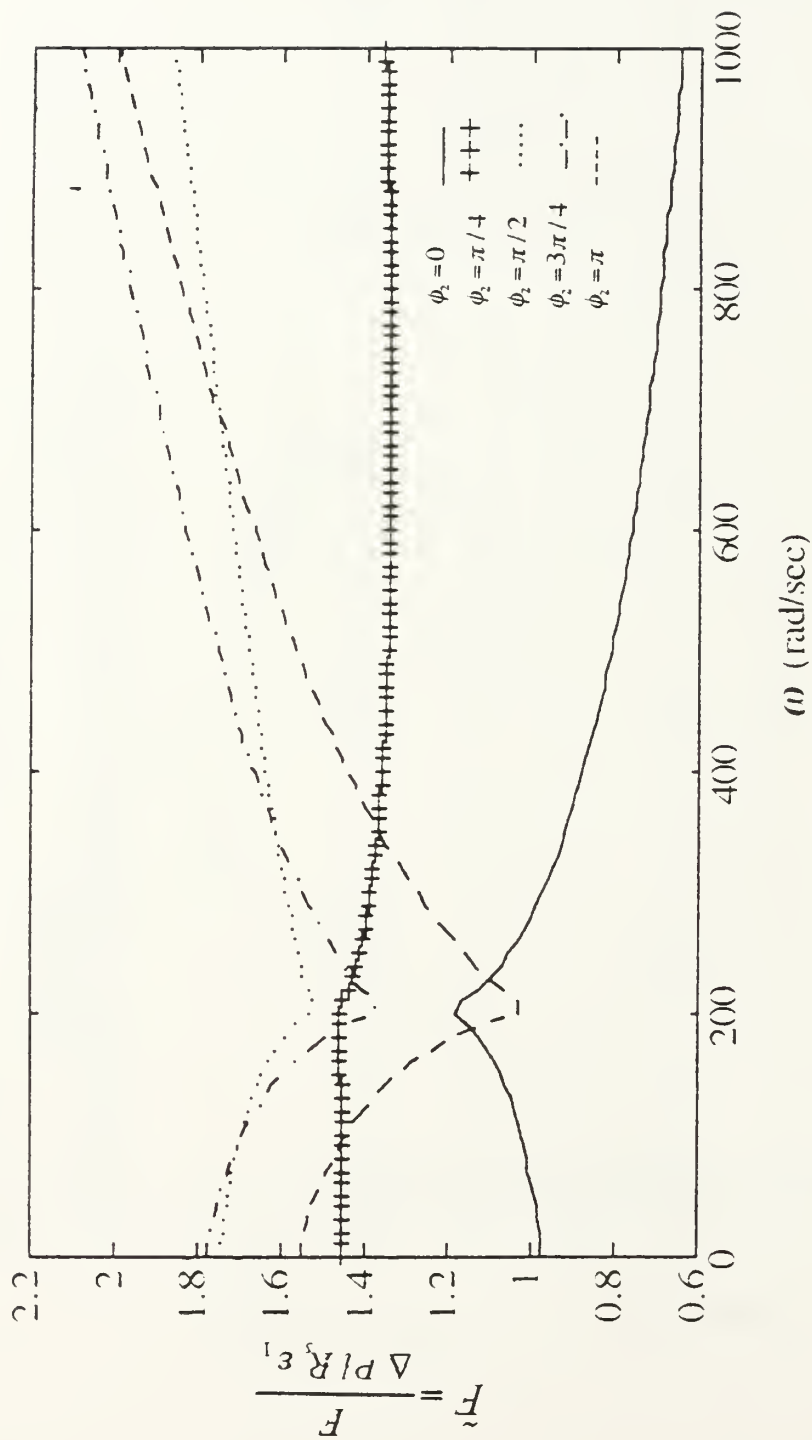
31

Figure 8. Force coefficient versus spin speed for a labyrinth with both front and back knife imperfections of the same size. The relative phase between the two imperfections is used as a parameter.

32

REFERENCES

1.   Thompson, B.D., Badgley, R.H., Raczkowski, R., 1989, "Methods and Procedures for Trim Balancing the LM2500 Marine Gas Turbine in the Test Cell and Aboard Ship", *The American Society of Mechanical Engineers* , Technical Report No 89-GT-318.

2.   Loewy, R.G., Piarulli, V.J., 1969, <u>Dynamics of Rotating Shafts</u> The Shock and Vibration Information Center United States Department of Defence, pp. 64-71.

3.   Muster, D., Stadelbauer, D.G., 1976, "Balancing of Rotating Machinery", <u>Shock & Vibration Handbook</u> Chapter 29, 2nd Edition, MaGraw Hill.

4.   Den Hartog, J.P., 1956, <u>Mechanical Vibrations</u> 4th Edition, McGraw Hill, pp. 281-283.

5.   Thompson, B.D., 1991, "Optimization of LM2500 Gas Generator and Power Turbine Trim Balance Techniques", *The American Society of Mechanical Engineers*, Technical Report No 91-GT-240.

6.   "Balancing Quality of Rotating Rigid Bodies", ISO 1940, 1st Edition, 1973-05-01, and ASA-STD 2 1975 (ANSI S2.19-1975).

7.   Kostyuk, A.G., 1972, "A Theoretical Analysis of the Aerodynamic Forces in the Labyrinth Glands of Turbomachines", <u>Teploenergetica</u> Vol. 19, No. 11, pp. 29-33.

8.   Iwatsubo, T., 1980, "Evaluation of Instability Forces in Labyrinth Seals in Turbines or Compressors", NASA CP-2133, pp. 139-169.

9.   Millsaps, K.T., 1992, "The Impact of Unsteady Swirling Flow in a Single Gland Labyrinth Seal on Rotordynamic Stability: Theory and Experiment", Ph. D. Dissertation, 1992, Massachusetts Institute of Technology.

10.   Millsaps, K.T., Martinez-Sanchez, M., 1993, "Dynamic Forces From Single Gland Labyrinth Seals: Part II - Upstream Coupling", International Gas Turbine Conference, Cincinnati, OH., 93-GT-322.

INITIAL DISTRIBUTION LIST

No. Copies

1. Defense Technical Information Center   2
   Cameron Station
   Alexandria, Virginia 22304-6145

2. Library, Code 52   2
   Naval Postgraduate School
   Monterey, California 93943-5002

3. Department Chairman, Code ME   1
   Department of Mechanical Engineering
   Naval Postgraduate School
   Monterey, CA 93943-5000

4. Professor K. Millsaps, Code ME-MI   5
   Department of Mechanical Engineering
   Naval Postgraduate School
   Monterey, CA 93943-5000

5. LT William C. Williston, Jr.   2
   287 Worden St.
   Portsmouth, RI 02871

6. Curricular Officer, Code 34   1
   Department of Naval Engineering
   Naval Postgraduate School
   Monterey, CA 93942-5000

7. Naval Sea Systems Command   1
   Mr. Dan A. Groghan
   Director, Engines Division (SEA S6X3)
   Washington D.C. 20362

GAYLORD S